Optics Communications 284 (2011) 3497–3503

Contents lists available at ScienceDirect

Optics Communications

journal homepage: www.elsevier.com/locate/optcom

White light interferometric detection of unpolarized light for complete Stokesmetric optical coherence tomography

Xue Liu [a,*], Shih C. Tseng [a], Renu Tripathi [a,c], Alexander Heifetz [a,d], Subramanian Krishnamurthy [a], M.S. Shahriar [a,b]

[a] Department of Electrical Engineering and Computer Science, Northwestern University, Evanston, IL 60208, United States
[b] Department of Physics and Astronomy, Northwestern University, Evanston, IL 60208, United States
[c] CREOSA, Department of Physics & Pre-Engineering, Delaware State University, Dover, DE 19901, United States
[d] Nuclear Engineering Division, Argonne National Laboratory, Argonne, IL 60439, United States

ARTICLE INFO

Article history:
Received 29 June 2010
Accepted 18 March 2011
Available online 6 April 2011

Keywords:
Optical coherence tomography
Polarization sensitive
Mueller matrix
Interferometric detection

ABSTRACT

Optical coherence tomography (OCT) relies on interference between a polarized reference and the target reflection. Thus, it has generally been impossible to detect any unpolarized part in the signal. Here, we demonstrate a scheme that overcomes this limitation. Using a combination of heterodyning and filtering, we realize a polarization-sensitive OCT system capable of measuring the full Stokes vector, including the depolarized part. Based on such a system, we perform full Stokesmetric imaging of different layers in a porcine tendon sample. The complete 4×4 backscattering Muellermetric images of one layer are acquired and investigated.

1. Introduction

Optical coherence tomography (OCT) is a relatively new technology for non-invasive biological imaging and non-destructive evaluation of materials [1–4]. The OCT techniques are based on low coherence interferometry (LCI) depth-scanning of the sample in the time domain [5]. The coherence length of the broadband light source determines the axial resolution of the OCT system. Currently, the OCT systems are able to discriminate the reflectivity of different depths within a sample typically at a micron-scale resolution [6–9].

Many biological tissues, such as tendon, bone, and tooth, exhibit birefringence because of their linear or fibrous structure, which alters the polarization state of light propagating in them [10,11]. For the purpose of acquiring the polarimetric signatures of biological tissues, several polarization-sensitive OCT (PSOCT) systems have been developed in recent years [12–17]. For example, de Boer et al. used the PSOCT system to generate images of thermally damaged tissue [12,13]. Hitzenberger et al. used the PSOCT to detect the phase retardation and fast axis orientation in chicken myocardium [14]. Everett et al. applied the PSOCT to the measurement of the birefringence of porcine myocardium [15]. Gang Yao et al. reported a PSOCT system aiming to yield the full set of Mueller matrix images of biological tissues and turbid media [16,17]. However, the PSOCT systems described in the refs. 16,17 are not capable of capturing the unpolarized part of the light reflected from the sample. Because of the coherent-detection scheme in their OCT system, an incorrect Degree of Polarization (DOP) of unity for the reflected light is measured for the solid sample. In order to calculate the DOP of light backscattered by liquid media, the authors assume that the total amount of light returned by the sample remains the same as the depth is varied. Although this assumption is not explicitly stated in the paper, it is the only plausible explanation for the results presented. The DOP of different layers, normalized to the DOP of the surface layer, is not the true DOP, since there is no evidence that the total amount of light reflected remains unchanged at various depths. Furthermore, even if this were the case for this particular sample, it does not represent a technique of general validity nor utility. What is needed is an ability to measure DOP without resorting to a depth scan and without having to make assumptions about the constancy of the total return signal from various depths.

To illustrate this inadequacy, consider the Poincare sphere shown in Fig. 1. The Poincare vector $\vec{P}$ is defined as $\vec{P} = Q\hat{q} + U\hat{u} + V\hat{v}$, where $\hat{q}$, $\hat{u}$ and $\hat{v}$ are the unit vectors of the three axes in the Poincare space. Q denotes the intensity difference between vertical and horizontal linear polarizations; U stands for the intensity difference between linear polarizations at $+45°$ and $-45°$, and V represents the intensity difference between left and right circular polarizations. In the Poincare space, we can define another vector, called the Poincare-Stokes vector, denoted as $\vec{S}_P$. This vector is parallel to $\vec{P}$, but has a length equal to the total intensity, I. The difference in the length between $|\vec{S}_P|$ and $|\vec{P}|$ characterizes the degree of depolarization. In the experiments of ref.'s 12–17, the system can only measure the magnitude and direction of $\vec{P}$. A system capable of performing complete

* Corresponding author. Tel.: +1 847 4917064.
E-mail address: xueliu2012@u.northwestern.edu (X. Liu).

0030-4018/$ – see front matter © 2011 Elsevier B.V. All rights reserved.
doi:10.1016/j.optcom.2011.03.054

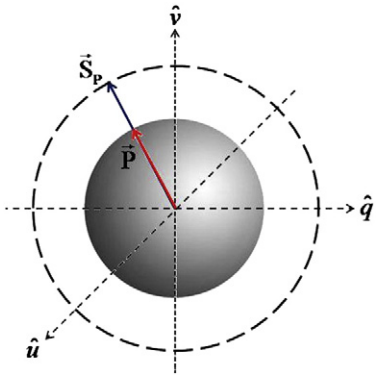

Fig. 1. Poincare–Stokes vector ($\vec{S}_P$) and Poincare vector ($\vec{P}$) representations in the Poincare space.

polarimetric imaging must be able to measure $\left|\vec{S}_P\right|$ in addition to $\vec{P}$. Explicitly, in some cases the reflected light from the sample is partially polarized. The information carried by the unpolarized light, represented by the gap between the surfaces of the Poincare sphere and the intensity sphere of radius $\left|\vec{S}_P\right|$, is missed by the PSOCT's. This incapability results in incomplete information in the measurement of the Mueller matrix in ref.'s 16 and 17.

In this paper, we demonstrate theoretically and experimentally the first PSOCT system capable of capturing the full Stokesmetric information of the sample reflection with the interferometry of unpolarized light using a combination of heterodyning and filtering techniques. We also apply such a PSOCT system to perform Stokesmetric imaging of different layers in a pork tendon sample. The full 4×4 Muellermetric images of one particular layer in the sample are investigated with the PSOCT system.

2. Configuration of the PSOCT system

Fig. 2 depicts the configuration of the heterodyned polarization-sensitive OCT system. A collimated beam from a broadband superluminescent diode (SLD) at a central wavelength of 845 nm is used as the light source. The linear polarizer (LP) selects a purely linear input state of the beam before being launched into the acousto-optic modulator (AOM). The unshifted beam at central frequency ω_b and the first order diffraction at central frequency ω_a are coupled into the two arms of a modified Michelson interferometer as the incident sample beam and the reference beam, respectively. A half-wave plate (HWP), followed by a quarter-wave plate (QWP) is placed on each arm of the Michelson interferometer to control the polarization state of the light. The probe beam is focused by a lens onto the sample mounted on a two-dimensional motorized translation stage, which can be driven for vertical and horizontal scans by computer programs. The back-scattered light from the sample recombines with the reference beam at a non-polarizing beam splitter (BS1). Only when the optical path difference between the two arms is within the coherence length of the SLD source do the two beams produce a beat note at the central frequency $\omega=\omega_a-\omega_b$ [18]. Thus, by moving M2 axially on the translation stage, one can select backscattered light from different depth layers of the sample to heterodyne with the reference beam. A photodetector is placed after BS1. The detected signal is sent into a high pass filter (HPF) followed by a mixer and a low pass filter (LPF).

Table 1
Intensities for different polarization states.

$I'_V=\frac{1}{2}(2ab_y)^2+(2ac)^2$
$I'_H=\frac{1}{2}(2ab_x)^2+(2ac)^2$
$I'_P=\frac{1}{2}\left(\left(\sqrt{2}ab_x\right)^2+\left(\sqrt{2}ac\right)^2+\left(\sqrt{2}ab_y\right)^2+\left(\sqrt{2}ac\right)^2\right)+\left(\sqrt{2}ab_x\right)\left(\sqrt{2}ab_y\right)\cos\delta_b$
$I'_M=\frac{1}{2}\left(\left(\sqrt{2}ab_x\right)^2+\left(\sqrt{2}ac\right)^2+\left(\sqrt{2}ab_y\right)^2+\left(\sqrt{2}ac\right)^2\right)-\left(\sqrt{2}ab_x\right)\left(\sqrt{2}ab_y\right)\cos\delta_b$
$I'_R=\frac{1}{2}\left(\left(\sqrt{2}ab_x\right)^2+\left(\sqrt{2}ac\right)^2+\left(\sqrt{2}ab_y\right)^2+\left(\sqrt{2}ac\right)^2\right)+\left(\sqrt{2}ab_x\right)\left(\sqrt{2}ab_y\right)\sin\delta_b$
$I'_L=\frac{1}{2}\left(\left(\sqrt{2}ab_x\right)^2+\left(\sqrt{2}ac\right)^2+\left(\sqrt{2}ab_y\right)^2+\left(\sqrt{2}ac\right)^2\right)-\left(\sqrt{2}ab_x\right)\left(\sqrt{2}ab_y\right)\sin\delta_b$

3. Theory

In this section we present a mathematical description of the heterodyned PSOCT system measurement of the Stokes vector of

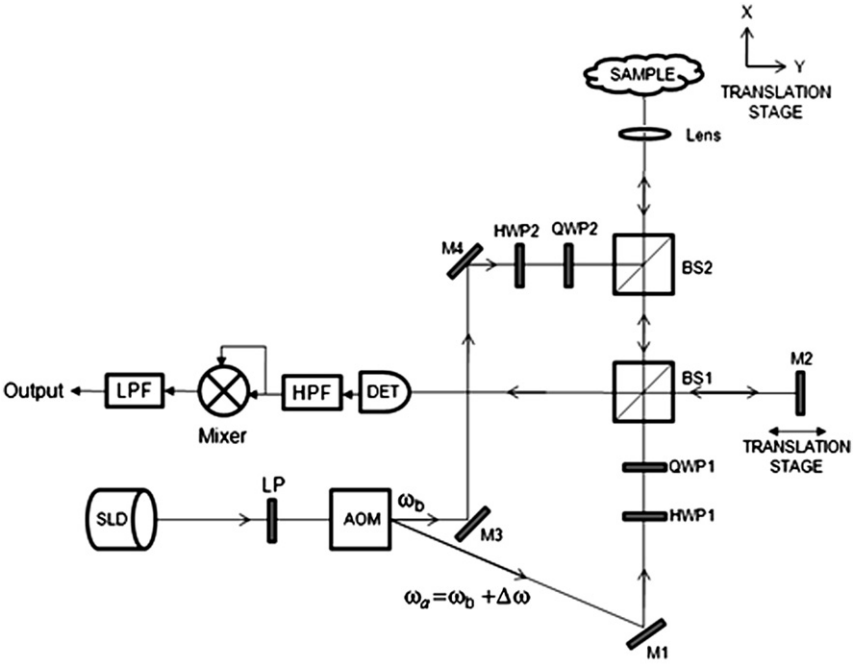

Fig. 2. Schematic diagram of the heterodyned PSOCT system. SLD: superluminescent diode; LP: linear polarizer; AOM: acousto-optic modulator; HWP: half wave plate; QWP: quarter wave plate; BS: beam splitter; M: mirror; DET: detector; HPF: high-pass filter; LPF: low-pass filter.

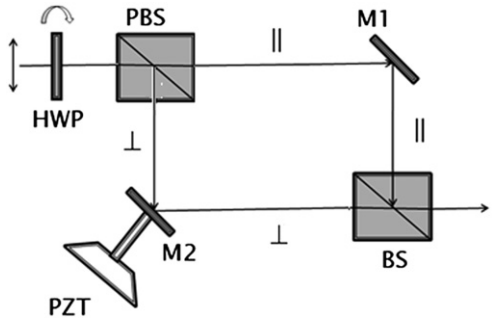

Fig. 3. Generating light of different degrees of depolarization. PBS: Polarization Beam Splitter; BS: Beam Splitter M: Mirror, PZT: Piezo Transducer.

depolarized reflection from the sample. The electric field of the reference beam, which for generality we describe as elliptically polarized, is represented by

$$\vec{E}_r = \left(a_x\hat{x} + a_y \exp(i\delta_a)\hat{y}\right) \exp(i\omega_a t)\beta(t) \quad (1)$$

where a_x and a_y are the amplitudes of the electric fields in the x- and y-directions, respectively. δ_a denotes the phase difference between the two components. ω_a is up-shifted 40 MHz by the AOM from the central frequency of the SLD in the current experimental setup. $\beta(t)$ represents the short coherence time of the laser source. For a broadband source such as the SLD, this can be expressed as $\beta(t) = \exp(i\phi(t))$ and has the following property [19]:

$$\langle \beta(t)\beta^*(t-\tau)\rangle = \exp(-\gamma|\tau|) \quad (2)$$

Here, the angular bracket denotes time averaging and γ^{-1} represents the coherence time of the source. For a pulsed source, $\beta(t)$ represents the pulse envelope, leading to a characteristic correlation time of the order of the pulse width.

The back-scattered light from the sample, with an unknown polarization state, is expressed by the superposition of two separate components as follows,

$$\vec{E}_s(t') = \left[\left(b_x\hat{x} + b_y \exp(i\delta_b)\hat{y}\right) + \left(c\exp(i\delta_{cx}(t'))\hat{x} + c\exp\left(i\delta_{cy}(t')\right)\hat{y}\right)\right] \times \exp(i\omega_b t') \exp(i\varphi_b(t'))\beta(t') \quad (3)$$

where $t' = t - \tau_d$ with τ_d being the time difference between the sample and reference arms. The first part of this expression denotes the polarized light, with b_x and b_y representing the amplitudes of the electric field in the x- and y- directions, respectively and δ_b denoting the phase difference between the two components. The second part denotes the depolarized component of backscattered object light, for which the mean amplitudes of electric field in the x- and y-directions are equal, denoted as c. $\delta_{cx}(t')$ and $\delta_{cy}(t')$ represent the randomly changing phases of the two components, which have a property similar to that of $\beta(t)$. Specifically,

$$\left\langle \exp\left(i\delta_\phi(t)\right) \exp\left(-i\delta_\phi(t-\tau)\right)\right\rangle = \exp\left(-\gamma_p|\tau|\right) \quad [\phi = cx \text{ or } cy] \quad (4)$$

so that γ_p represents the bandwidth of depolarization. $\varphi_b(t)$ denotes the relative phase fluctuation of the object beam with respect to the reference beam, due to the environment of the experiment, for example. Here, we have ignored the reflected light at frequency ω_a since the heterodyning process readily eliminates it.

According to Eq. (3), the maximum heterodyned signal for a specific layer occurs when the light reflected by the layer traverses the same optical path length as the light in the reference arm, i.e., $\tau_d = 0$. In such a case, the total intensity of the signal seen by the detector, denoted as I', can be written as

$$\begin{aligned} I' = \left\langle \left|\vec{E}_r + \vec{E}_s\right|\right\rangle &= a_x^2 + b_x^2 + a_y^2 + b_y^2 + 2c^2 + \langle 2a_x b_x \cos(\omega t - \varphi_b(t))\rangle \\ &+ \left\langle 2a_y b_y \cos(\omega t - \varphi_b(t) + \delta_a - \delta_b)\right\rangle + \langle 2a_x c \cos(\omega t - \delta_{cx}(t) - \varphi_b(t))\rangle \\ &+ \left\langle 2a_y c \cos\left(\omega t + \delta_a - \delta_{cy}(t) - \varphi_b(t)\right)\right\rangle + \langle 2b_x c \cos(-\delta_{cx}(t))\rangle \\ &+ \left\langle 2b_y c \cos\left(\delta_b - \delta_{cy}(t)\right)\right\rangle \end{aligned} \quad (5)$$

where $\omega = \omega_a - \omega_b$ is the central frequency of the heterodyned signal. The angular brackets imply time-averaging over the detection process. Since $\varphi_b(t)$, $\delta_{cx}(t)$ and $\delta_{cy}(t)$ are randomly varying phases, the last two terms in Eq. (5) averages to 0 provided the detection bandwidth is much smaller than the depolarization bandwidth γ_p.

To measure the Stokes vector of the reflected object beam, we process the detected signal through the following filtering steps. First, we use the HPF to extract the beat note at frequency ω by filtering out the DC signal and noise. We assume that the low frequency cutoff for the HPF occurs at a frequency much larger than the bandwidth of any low-frequency system noise. The signal after the HPF becomes

$$\begin{aligned} I' &= 2a_x b_x \cos(\omega t - \varphi_b(t)) + 2a_x c \cos(\omega t - \delta_{cx}(t)) \\ &+ 2a_y b_y \cos(\omega t - \varphi_b(t) + \delta_a - \delta_b) + 2a_y c \cos\left(\omega t + \delta_a - \delta_{cy}(t)\right) \end{aligned} \quad (6)$$

The signal is then squared by a mixer, which results in new DC components as well as sinusoidal signals at frequency 2ω The DC part

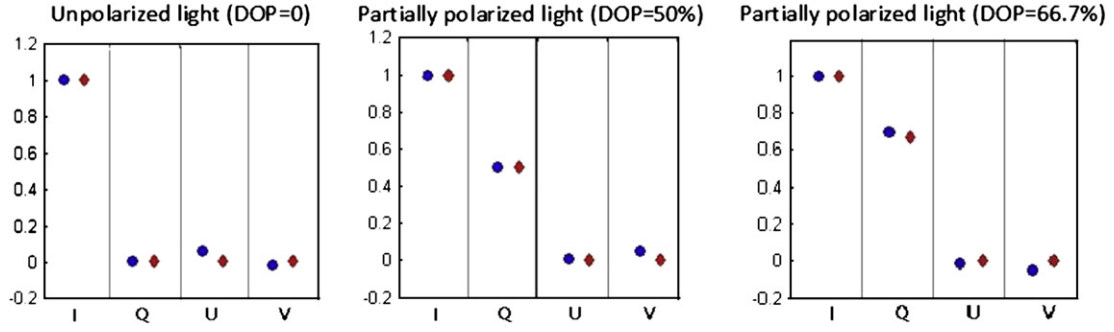

Fig. 4. Theoretical and experimentally measured Stokes parameters for lights of different degrees of depolarization using the heterodyned PSOCT system. ♦ stands for the theoretical value, ■ stands for the measured value.

Table 2
The DOP and proportion of polarization components of Stokes vector for different layers.

	DOP (%)	$\|Q\|^2/I^2$ (%)	$\|U\|^2/I^2$ (%)	$\|V\|^2/I^2$ (%)
Layer I	68.73	8.12	5.47	33.15
Layer II	55.10	13.77	7.60	8.98
Layer III	35.57	2.80	2.09	7.76

of the signal is extracted by the LPF with a bandwidth lower than the depolarization bandwidth γ_p. The final output from the LPF is

$$I' = \frac{1}{2}(2a_x b_x)^2 + \frac{1}{2}\left(2a_y b_y\right)^2 + \frac{1}{2}(2a_x c)^2 + \frac{1}{2}\left(2a_y c\right)^2 + (2a_x b_x)\left(2a_y b_y\right)\cos(\delta_a - \delta_b) \tag{7}$$

Eq. (7) shows that the output signal depends on the polarization states of both the sample reflection and the reference beam. Here a_x, a_y and δ_a are controllable parameters for the reference arm. The four unknown quantities, b_x, b_y, c and δ_b, fully determine the Stokes vector of the reflected beam through the following expression [20].

$$\vec{S}_r = \left[b_x^2 + b_y^2 + 2c^2, b_x^2 - b_y^2, 2b_x b_y \cos\delta_b, 2b_x b_y \sin\delta_b\right]^T \tag{8}$$

In principle, b_x, b_y, c and δ_b can be determined by analyzing the OCT signal generated by the sample reflection and the reference beam of four arbitrary linearly independent polarizations.

To illustrate this process systematically, we define first a convenient set of input polarization states. These are *vertical, horizontal, linear*45°, *linear* −45°, *right circular and left circular*, denoted as V, H, P, M, R and L, respectively. The intensities of the output signal for different reference beams calculated from Eq. (7) are summarized in Table 1. Here, we have defined $a = \sqrt{I_r}$ for notational brevity where I_r denotes the intensity of the reference beam.

Based on the results in Table 1, the four parameters that determines the Stokes vector in Eq. (8) are calculated as follows,

$$b_x = \left[(I'_H - I'_V) + \sqrt{(I'_H - I'_V)^2 + (I'_P - I'_M)^2 + (I'_R - I'_L)^2}\right]^{\frac{1}{2}} \tag{9.a}$$

$$b_y = \left[-(I'_H - I'_V) + \sqrt{(I'_H - I'_V)^2 + (I'_P - I'_M)^2 + (I'_R - I'_L)^2}\right]^{\frac{1}{2}} \tag{9.b}$$

$$c = \left[2I'_H - (I'_H - I'_V) - \sqrt{(I'_H - I'_V)^2 + (I'_P - I'_M)^2 + (I'_R - I'_L)^2}\right]^{\frac{1}{2}} \tag{9.c}$$

$$\delta_b = \tan^{-1}\left(\frac{I'_R - I'_L}{I'_P - I'_M}\right) \tag{9.d}$$

The Stokes vector can be simply expressed as

$$\vec{S}_r = \left[I'_H + I'_V, I'_H - I'_V, I'_P - I'_M, I'_R - I'_L\right]^T \tag{10}$$

However, due to the linear dependence (Note that $I'_H + I'_v = I'_P + I'_M = I'_R + I'_L$.), Eq. (10) can also be expressed by four linearly independent elements from the reference set, e.g.,

$$\vec{S}_r = \left[I'_H + I'_V, I'_H - I'_V, 2I'_P - I'_H - I'_V, 2I'_R - I'_H - I'_V\right]^T \tag{11}$$

Thus, by using four of the six inputs (e.g., H, V, P and R), we can determine $\vec{S}_r$.

The polarization dependent scattering property of the sample can be characterized fully by determining all element of the Mueller matrix, M, which relates the Stokes vector of the object beam ($\vec{S}_o$) to the Stokes vector of the scattered light ($\vec{S}_r$):$\vec{S}_r = M\vec{S}_o$. In order to

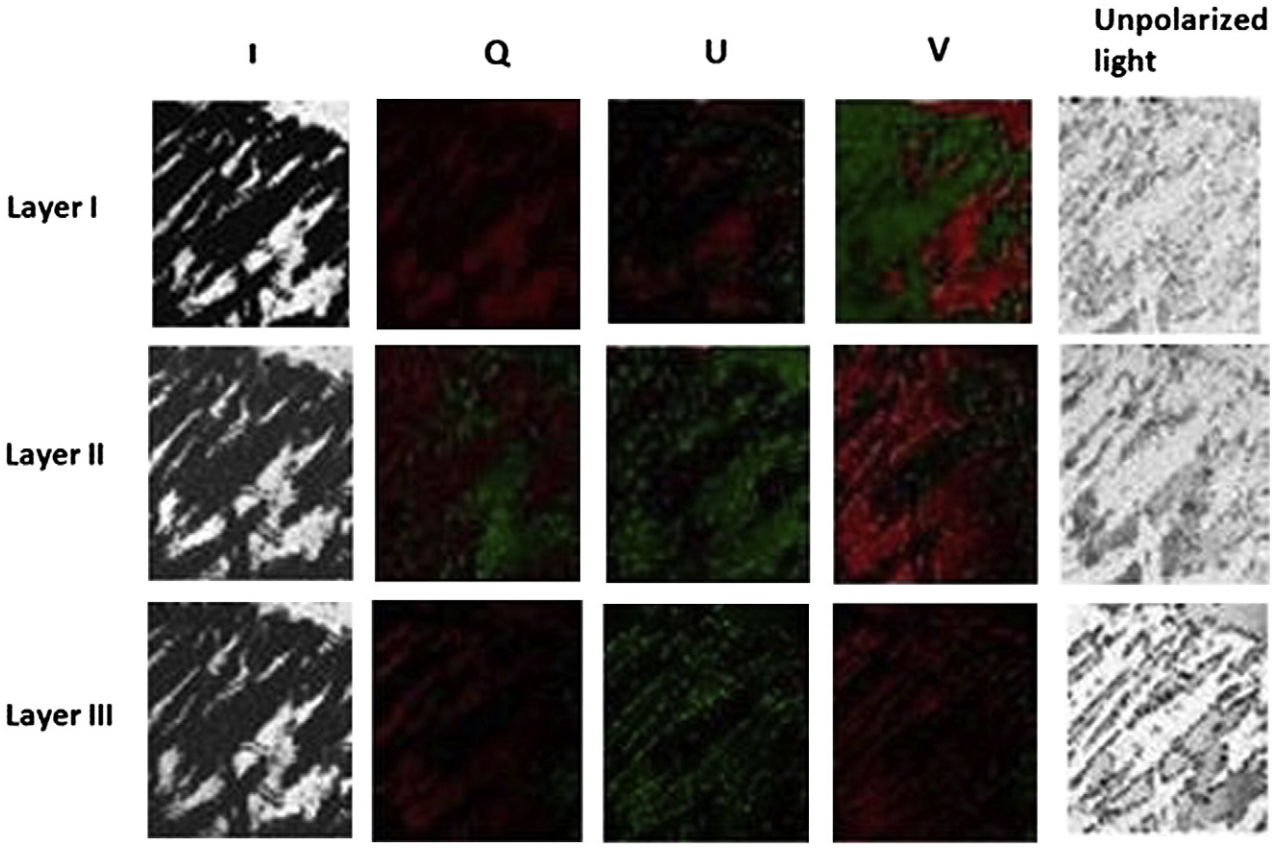

Fig. 5. Stokesmetric imaging of different layers within the porcine muscle sample.

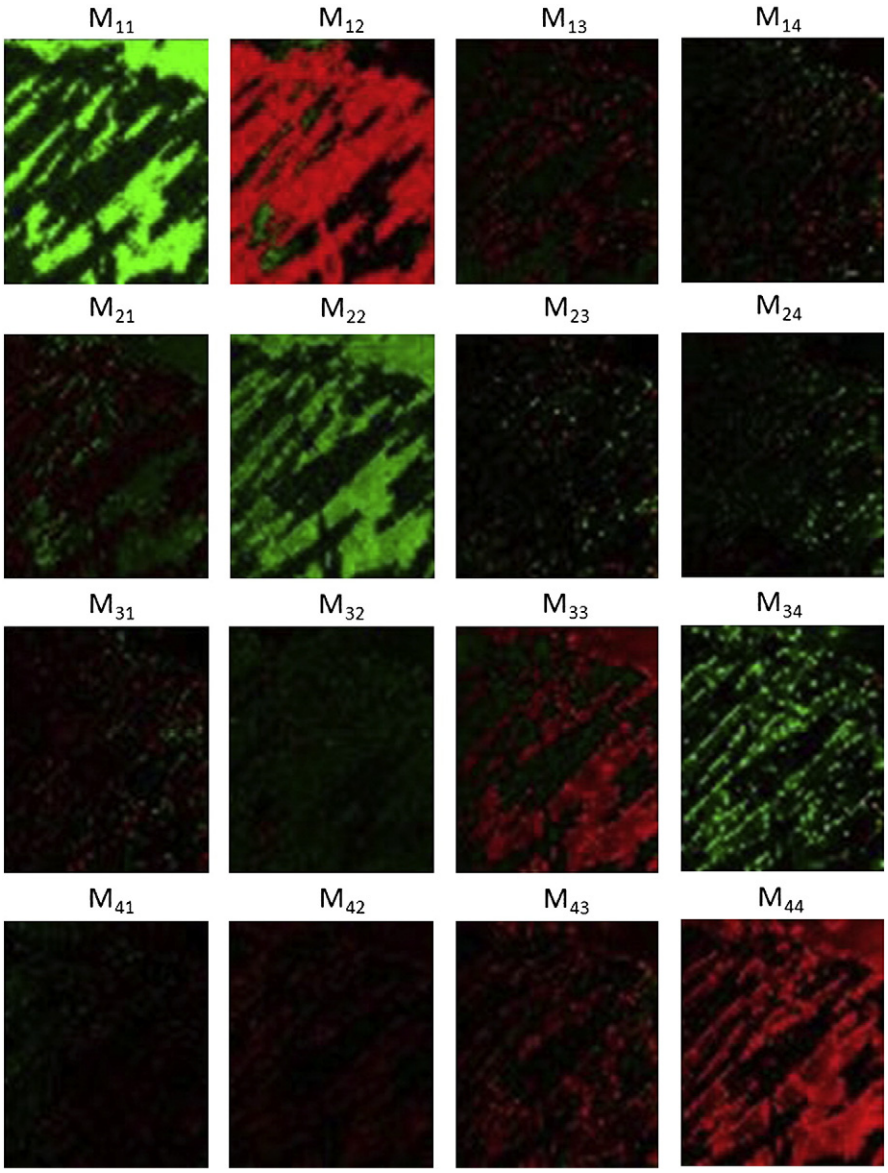

Fig. 6. Backscattering Mueller matrix images of the porcine tendon sample.

determine the elements of M, it is necessary to vary the polarization of the object beam through four different orthogonal states. This can be accomplished by rotating HWP2 and QWP2 in Fig. 2. A detailed analysis shows that the full Mueller matrix is given by

$$M=\begin{bmatrix} I'_{HH}+I'_{HV}+I'_{VH}+I'_{VV}I'_{HH}+I'_{HV}-I'_{VH}-I'_{VV}I'_{PH}+I'_{PV}-I'_{MH}-I'_{MV}I'_{RH}+I'_{RV}-I'_{LH}-I'_{LV} \\ I'_{HH}-I'_{HV}+I'_{VH}-I'_{VV}I'_{HH}-I'_{HV}-I'_{VH}+I'_{VV}I'_{PH}-I'_{PV}-I'_{MH}+I'_{MV}I'_{RH}-I'_{RV}-I'_{LH}+I'_{LV} \\ I'_{HP}-I'_{HM}+I'_{VP}-I'_{VM}I'_{HP}-I'_{HM}-I'_{VP}+I'_{VM}I'_{PP}-I'_{PM}-I'_{MP}+I'_{MM}I'_{RP}-I'_{RM}-I'_{LP}+I'_{LM} \\ I'_{HR}-I'_{HL}+I'_{VR}-I'_{VL}I'_{HR}-I'_{HL}-I'_{VR}+I'_{VL}I'_{PR}-I'_{PL}-I'_{MR}+I'_{ML}I'_{RR}-I'_{RL}-I'_{LR}+I'_{LL} \end{bmatrix} \quad (12)$$

where the first/second letter of the subscript denotes the polarization state of the incident object/reference beam, respectively.

4. Results

4.1. Verification of the PSOCT system with single point light source

To test the heterodyned PSOCT system, we generate partially polarized light using the configuration shown in Fig. 3, and use it as a controlled form of sample reflection. The linear vertically polarized input light, after being rotated by a HWP, is split by a polarization beam splitter (PBS) into horizontally and vertically polarized components. The relative phase difference between these two paths is randomly changed between $-\pi$ and π by a mirror mounted on a Piezo transducer (PZT), which is driven by a noise signal produced by a computer using a random number generator. The two polarization components are recombined at a regular BS. When the amplitudes of the two components are equal, fully unpolarized light is achieved. We can also change the ratio between the vertical and horizontal components by rotating the HWP, thus getting partially polarized light of different degrees of depolarization. Fig. 4 shows the theoretical and measured Stokes parameters for unpolarized (DOP = 0) and two cases of partially polarized light (DOP = 50% for the first case and DOP = 66.7% for the second). The average deviation of the measured Stokes parameters using the heterodyned PSOCT system is 2.59% from the theoretical values, which may be attributable to the imprecision in orientating the optical components and the inherent intensity noise in the detection process.

4.2. Stokesmetric imaging of biological sample

We applied the PSOCT system to perform Stokesmetric imaging of layers at varying depths in a porcine tendon sample. The imaged area

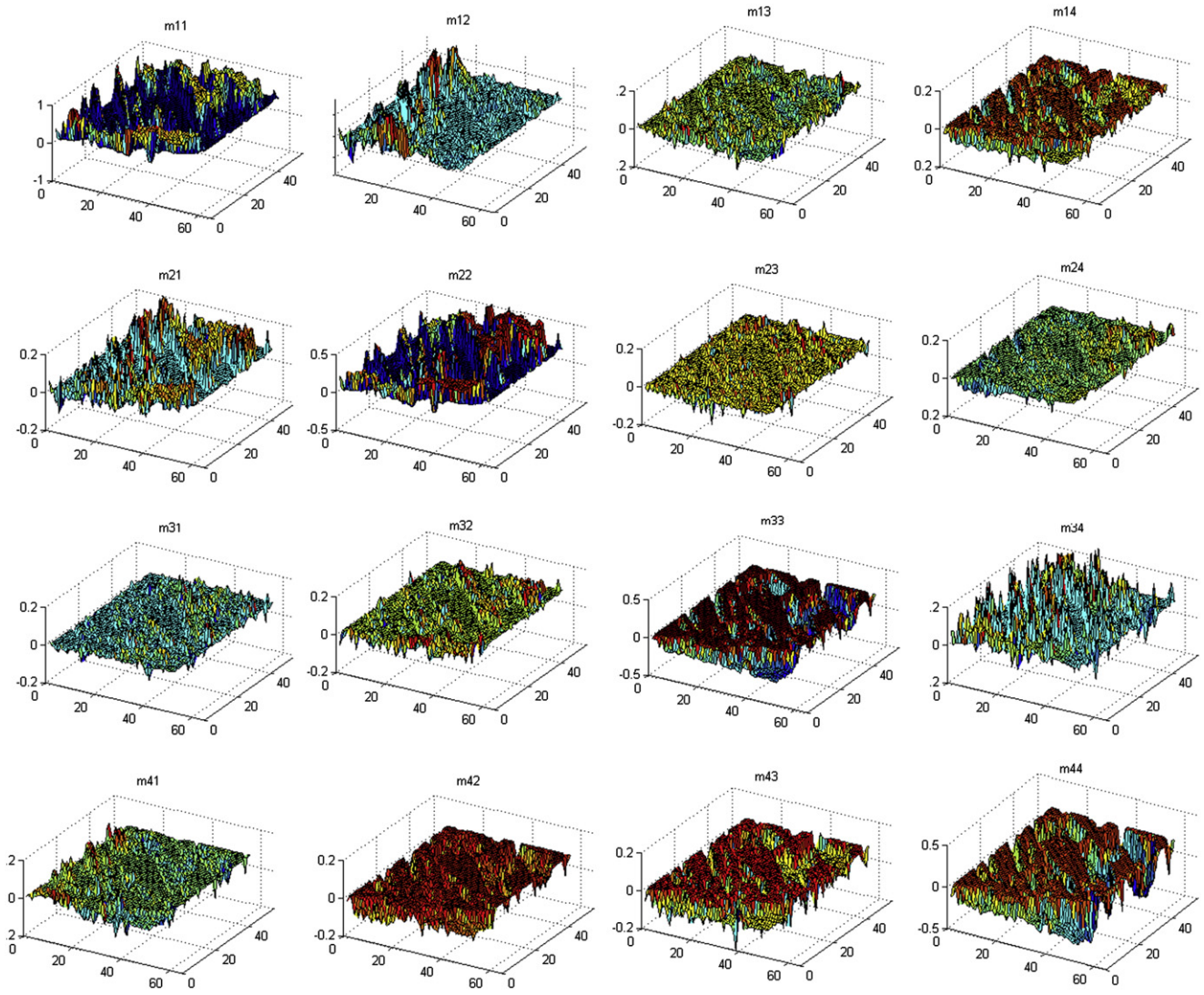

Fig. 7. 3-D structure images of each Mueller matrix element of the tendon sample.

(2.4 mm × 2.0 mm) of the sample is chosen to consist of both muscle and fat. The incident object beam is set to be left-circularly polarized. The beam has a diameter of 40 μm after being focused by the lens. Two-dimensional image scanning is performed to three layers of different depths in the sample: (I) the surface (II) the sub-surface layer 30 μm under a surface and (III) the sub-surface layer 50 μm under a surface. The Stokes vector of backscattered light collected at each scanning step, treated as a pixel, is analyzed according to Eq. (1) and plotted in Fig. 2. For *Q, U* and *V,* green and red colors stand for positive and negative values, respectively. The fifth column shows the unpolarized part of the light.

In Table 2, we present an analysis of this data for signals integrated over the whole image. Note that these numbers very nearly satisfy the relation that $\mathrm{DOP} = \left(\frac{|Q|^2 + |U|^2 + |V|^2}{I^2}\right)^{1/2}$. As can be seen from Table 2, the DOP decreases as the depth of penetration in the sample increases. The table also shows that each layer couples the original polarization, which is purely circular, into linear polarizations to different extents. More importantly, as can be seen from Fig. 5, the signs of the images for the Q and U elements, representing the directions of the linear polarizations, differ from one another for the three layers. As shown in ref. [21] and ref. [22], the change of the polarization of light in a medium has a dependence on the geometrical and optical properties of the particles. The differences of signs and values of the reflected Q and U images of the three layers may imply different compositions of particles.

4.3. Backscattering Muellermetric imaging of biological sample

We use the PSOCT to obtain the Muellermetric images of Layer III of the porcine tendon sample. In keeping with Eq. (12), thirty-six heterodyned images for different polarization combinations of the incident object beam and the reference beam are recorded. The sixteen images corresponding to the 4×4 backscattered Mueller matrix are computed by linear combinations of the raw images according to Eq. (12). These are shown below in Fig. 6 where M_{ij} represents the *i*th row and the *j*th column of the Mueller matrix. Here again, green and red colors represent the positive and negative values, respectively.

Fig. 6 leads to some important observations about the backscattering Mueller matrix of the layer of the tendon sample. (1) The diagonal elements have much bigger magnitude than the off-diagonal ones. Strong morphological patterns can be observed in the diagonal images. M_{33} and M_{44} exhibit negative values due to the π phase-shift produced at reflection. (2) For the off-diagonal elements, M_{21}, M_{31} and M_{41} have near-zero amplitudes, which agrees with the fact that the sample can hardly convert unpolarized light into polarized light. The elements M_{34} and M_{43}, representing the coupling between

circularly polarized light and 45° linearly polarized light, have significantly larger values than the other off-diagonal elements. The anti-symmetry (equal amplitude with opposite signs) of M_{34} and M_{43} indicate the birefringence produced by the sample. The phase delay between the horizontal and vertical polarizations turns the incident left-circularly polarized light into −45° linearly polarized light, which is readily shown on pictures in the third row of Fig. 5. In addition, some dotted patterns are observed on M_{34}. As we know, different particles cluster at different locations. The discontinuity may imply compositional variation on the layer.

The 3-D Muellermetric images of Layer III are plotted in Fig. 7. The variations in spatial structure of each elementary image can be readily observed in such pictures. The knowledge of the Mueller matrix of the sample enables us to determine the polarization state of back-scattered light from any point on the sample for any arbitrary probe beam. On the other hand, the 16 elements of the Mueller matrix fully characterize the polarimetric signature of the tissue, thus can be used for sample characterization and identification.

5. Conclusion

In this paper, we developed and demonstrated measurements of the Stokes vectors of lights of different degrees of depolarization with a PSOCT system based on heterodyning and filtering techniques. The calculated Stokes parameters from the measurement agree well with the theoretical values for all cases. The complete 4×4 backscattering Muellermetric images of a porcine tendon sample are acquired and investigated using such a system.

Acknowledgements

This work is supported in part by AFOSR grant #FA9550-06-1-0466, NASA Grant #NNX09AU90A, DOE grant #DE-AC02-06CH11357 and NSF Crest grant #0630388.

References

[1] M.R. Hee, D. Huang, E.A. Swanson, J.G. Fujimoto, J. Opt. Soc. Am. B 9 (1992) 903.
[2] D. Huang, E.A. Swanson, C.P. Lin, D. Huang, E.A. Swanson, C.P. Lin, J.S. Schuman, W.G. Stinson, W. Chang, M.R. Hee, T. Flotte, K. Gregory, C.A. Puliafito, J.G. Fujimoto, Science 254 (1991) 1178.
[3] A.F. Fercher, J. Biomed. Opt. 1 (1996) 157.
[4] M. Brezinski, Optical Coherence Tomography: Principles and Applications, Elsevier, Burlington, 2006.
[5] J.M. Schmitt, IEEE J. Sel. Top. Quantum Electron. 5 (1999) 1205.
[6] J.G. Fujimoto, Nat. Biotechnol. 21 (2003) 1361.
[7] Wolfgang Drexler, J. Biomed. Opt. 9 (2004) 47.
[8] W. Drexler, U. Morgner, F.X. K¨artner, C. Pitris, S.A. Boppart, X.D. Li, E.P. Ippen, J.G. Fujimoto, Opt. Lett. 24 (1999) 1221.
[9] Ding Zhihua, Ren Hongwu, Zhao Yonghua, J. Stuart Nelson, Chen Zhongping, Opt. Lett. 27 (2002) 243.
[10] Michael R. Hee, David Huang, Eric A. Swanson, James G. Fujimoto, J. Opt. Soc. Am. B 9 (1992) 903.
[11] Richard C. Haskell, Francis D. Carlson, Paul S. Blank, Biophys. J. 56 (1989) 401.
[12] J.F. de Boer, T.E. Milner, J.S. Nelson, Opt. Lett. 24 (1999) 300.
[13] J.F. deBoer, S. Sriniwas, A. Malekafzali, Z.P. Chen, J.S. Nelson, Opt. Exp. 3 (1998) 212.
[14] Christoph K. Hitzenberger, Erich Götzinger, Markus Sticker, Michael Pircher, Adolf F. Fercher, Opt. Exp. 9 (2001) 780.
[15] M.J. Everett, K. Schoenenberger, B.W. Colston Jr., L.B. Da Silva, Opt. Lett. 23 (1998) 228.
[16] G. Yao, L.V. Wang, Opt. Lett. 24 (1999) 537.
[17] Shuliang Jiao, Gang Yao, Lihong V. Wang, Appl. Opt. 39 (2000) 6318.
[18] The part of light at ω_a, reflected from the sample, does not contribute to the observed signal because of path length mismatch.
[19] See, for example. M. Sargent, M.O. Scully, W.E. Lamb, Laser Physics, Addison-Wesley, London, 1974, p. 86.
[20] D. Goldstein, Polarized Light, 2nd Ed, CRC Press, New York, 2003.
[21] M.I. Mishchenko, J.W. Hovenier, Opt. Lett. 20 (1995) 1356.
[22] Tuchin Valery, Tissue Optics, SPIE press, 2000.